Pergamon

Int. J. Heat Mass Transfer. Vol. 40, No. 18, pp. 4425–4435, 1997

Printed in Great Britain
0017-9310/97 $17.00+0.00

PII: S0017-9310(97)00066-5

Melting heat transfer characteristics of a horizontal ice cylinder immersed in quiescent saline water

M. YAMADA, S. FUKUSAKO,† T. KAWANAMI and C. WATANABE

Division of Mechanical Science, Graduate School of Engineering, Hokkaido University, N-13 W-8, Kita-ku, Sapporo 060, Japan

(*Received* 4 *September* 1996 *and in final form* 28 *January* 1997)

Abstract—Experiments were performed to determine the effect of salinity level on the melting heat transfer characteristics of a horizontal ice cylinder immersed in quiescent saline water. Emphasis was placed on interpreting the heat transfer mechanism which dominates the solid–liquid interface situation. Measurements were carried out for saline water of 0.5–3.5 wt% in salinity, while the ambient temperature ranged from 1.8 to 24.0°C. Flow visualization was employed to investigate the transient flow patterns and corresponding solid–liquid interface locations. It was found that the flow patterns around the ice cylinder were a strong function of the saline water concentration, which then considerably affected the local heat transfer coefficient along the melting ice cylinder. © 1996 Elsevier Science Ltd.

1. INTRODUCTION

Melting heat transfer has been a subject of intensive experimental and analytical investigation for many years, because melting phenomena are extensively encountered in nature and a variety of technologically important processes. Useful summaries of the works have been published [1–4]. Although the basic transport mechanism cannot be regarded as fully understood, the fact remains that the melting heat transfer characteristics of the single component system for a monotonous configuration may be predicted with adequate certainty. However, there remain a variety of unsolved melting problems, to which the previous basic data characterizing the processes cannot be applicable. One such problem is the melting characteristics of ice blocks in seawater, in which a couple of heat and concentration transfers occur along with phase change.

The melting of a glacier in the sea has an influence on both the temperature and concentration fields in the ocean which, consequently, may result in considerable effects on the biological systems of the ocean [5–8] and on the climate by earth-scale. The melting of ice blocks in the sea is, thus, of great importance for both biological oceanography and meteorology. The glaciers in the Arctic and the icebergs in the Antarctic contain a much smaller salt concentration than the sea ice does, which indicates that the melting characteristics of the ice blocks in the sea may be expected to be somewhat different from those of the common sea ice.

A number of the experimental and analytical studies were reported on the melting of ice blocks in saline water [9–18]. All of the aforementioned investigations pertaining to melting of ice blocks in the saline water were mainly concerned with transport phenomena along the vertical or horizontal ice surface. Recently, melting characteristics of a horizontal, circular ice cylinder, as well as both downward- and upward-facing ice plates immersed in quiescent saline water [19–21], were extensively determined.

The primary objective of the present paper is to report the effect of ambient salinity level on the melting heat transfer characteristics of a horizontal ice cylinder immersed in quiescent saline water. The ambient salinity level was varied from 0.5 to 3.5 wt% for ambient temperatures ranging from 1.8 to 24.0°C. Photographs of flow visualization for free convection flow adjacent to the melting ice surface, obtained by illuminating suspended particles in saline water, are presented. Local/average heat transfer coefficient was determined using ice profiles measured from photographs of the ice layer. The experimental results for the average Nusselt numbers are compared with the experimental data from a melting ice cylinder immersed in quiescent pure water [22, 23].

2. EXPERIMENTAL APPARATUS AND PROCEDURES

2.1. *Experimental apparatus*

A schematic diagram of the experimental apparatus is shown in Fig. 1. The apparatus consists basically of a test section, heat exchangers, coolant-circulating system and associated instrumentation. The rectangular test vessel measures 200 mm wide, 730 mm

† Author to whom correspondence should be addressed.

NOMENCLATURE

A_ϕ local heat transfer surface [m^2]
a thermal diffusivity [m^2 s^{-1}]
D diameter of ice cylinder [m]
$(db/dt)_\phi$ melting velocity perpendicular to ice surface [m s^{-1}]
g gravitational acceleration [m s^{-2}]
h_ϕ local heat transfer coefficient defined in equation (2) [W m^{-2} K^{-1}]
h_m average heat transfer coefficient defined in equation (3) [W m^{-2} K^{-1}]
L latent heat of fusion per unit mass [J kg^{-1}]
Nu_m average Nusselt number defined in equation (7)
Nu_m^* modified Nusselt number defined in equation (8)
Ra Rayleigh number defined in equation (9)
S concentration of salt [wt%]
T temperature [°C]
ΔT temperature difference ($= T_\infty - T_o$) [°C]
t time [s].

Greek symbols
λ thermal conductivity [W m^{-1} K^{-1}]
ν kinematic viscosity [m^2 s^{-1}]
ρ density [kg m^{-3}]
ϕ angle measured from top of cylinder [deg].

Subscripts
fp fusion temperature of solution
i ice
in initial
o ice surface
sp freezing temperature of solvent in solution
∞ ambient.

high and 800 mm long, and is made of transparent lucite plate of 15 mm in thickness, except for a double-pane glass in the front.

A copper concentric cylinder (28.6 mm o.d., wall thickness 1.5 mm and length 200 mm), which was utilized to make a bubble-free ice cylinder, was placed at the middle of the vessel (450 mm distance from the bottom). As depicted in Fig. 2, a coiled spring was inserted in the annular space to promote turbulence of the coolant (a mixture of ethylene glycol and water) circulating in the cylinder and, thus, to obtain high heat transfer rates. In addition, the temperature-regulated coolant was injected intensively from many holes (3 mm diameter) drilled through the inner cylinder wall. The coolant was circulated at a high velocity between the cylinder and a temperature-regulated bath. The uniformity of the cylinder surface temperature was confirmed as the difference between the inlet and outlet temperatures of the coolant in the cylinder were within about 0.1°C of each other.

The surface temperature of the cylinder was measured at 45° intervals from the top of the cylinder, using 10 chromel–alumel thermocouples of 0.1 mm diameter. Ambient saline-water temperature was also measured at 50-mm intervals from the bottom of the test vessel using 13 chromel–alumel thermocouples of 0.1 mm diameter. The salinity of the water was estimated by use of a salinity meter (Yokogawa SC8211-J).

The coolant-circulating system consists of a refrigerator (3.5 kW), coolant bath (400 l), an agitator and two centrifugal pumps. A mixture of ethylene–glycol and water was adopted as the coolant. The flow pattern for free convection flow around the ice cylinder was visualized by mixing an aluminum powder of about few microns in average diameter into the saline water. A He–Ne laser was utilized as the light source, which was appropriately expanded to two-dimensional light sheet by use of a cylindrical lens. The length of the exposures for the streak photographs was between 20 and 40 s.

2.2. *Experimental procedures*

First, a bubble-free ice cylinder was made in the test bath filled with pure water by injecting air bubbles against the cooled tube from the air nozzles placed at the bottom of the test bath. This air bubble flow scribes off the small air bubbles, which were formed on the solidification interface and were captured into the ice layer, in order to prevent these small air bubbles from making the ice layer unclear. In this process, the thermocouples (0.1 mm diameter chromel–alumel supported, respectively, by stainless tubes) were embedded in the ice layer formed around the cooled tube at 5-mm intervals.

After reaching a prescribed diameter of ice cylinder (85–90 mm in diameter), the pure water in the test bath was discharged and then temperature-regulated saline water was introduced into the test bath to replace the pure water. Saline water (a mixture of pure water and pure NaCl) of 0.5–3.5 wt% in salinity level was adopted as a testing liquid. Special care was taken in introducing the saline water. The saline water was introduced quite slowly through three pipes (20 mm in diameter), which were connected to the bottom of the test bath and whose nozzles were arranged horizontally along the bottom surface to minimize the effect of the undesirable fluid-spouting. When the

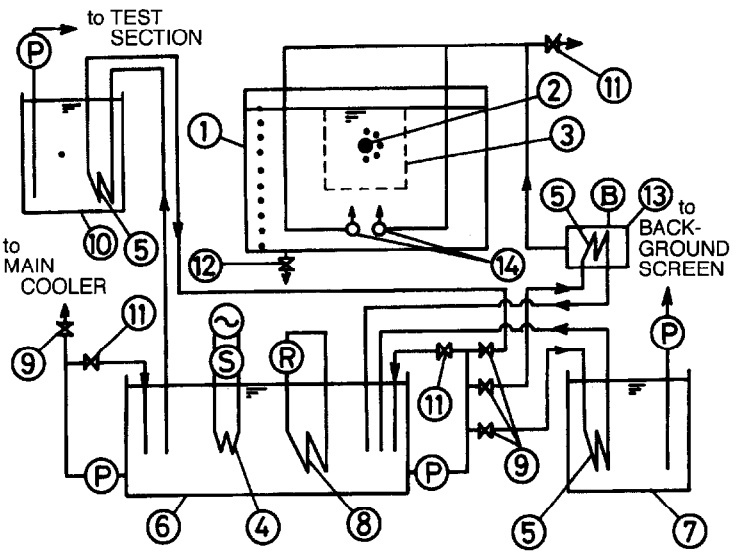

① TEST SECTION
② MAIN COOLER
③ BACKGROUND SCREEN
④ HEATER
⑤ HEAT EXCHANGER
⑥ MAIN BRINE TANK
⑦ SUB BRINE TANK
⑧ EVAPORATOR
⑨ CONTROLLING VALVE
⑩ SALINE WATER TANK
⑪ BYPASS VALVE
⑫ DRAIN VALVE
⑬ AIR COOLER
⑭ AIR NOZZLE
Ⓟ PUMP
Ⓡ REFRIGERATOR
Ⓢ SLIDAC
Ⓑ BLOWER
• THERMOCOUPLES

Fig. 1. Schematic diagram of experimental apparatus.

liquid level reached just below the bottom of the horizontal ice cylinder, the liquid supply was stopped for a few minutes. Then the liquid supply was restarted so that the liquid would arrive at the prescribed level above the ice cylinder. Data runs were carried out for the ambient saline-water temperatures ranging from 1.8 to 24.0°C.

3. DATA REDUCTION

3.1. *Ambient temperature and salinity*

The model studied in the present experiment is melting heat transfer around a horizontal ice cylinder immersed in quiescent liquid possessing both uniform temperature and uniform salinity. To maintain uniform far-field conditions, the size of the saline-water bath was made large. Any artificial heating of liquid and regulating of salinity during a course of the melting were not carried out to avoid additional undesirable effects that would be introduced due to such handling. Through the present experiment it was observed that the maximum variation (relative ratio of variation to initial value) for the ambient temperature was about 5.5%, while that for ambient salinity was about 3.4% during a course of the melting.

3.2. *Determination of heat transfer coefficient*

A local thermal energy balance at the melting surface of the cylinder, which is at the fusion temperature, can be written as:

$$\rho_i L(\mathrm{d}b/\mathrm{d}t)_\phi = h_\phi(T_\infty - T_o). \quad (1)$$

At any angular location ϕ, the local heat transfer coefficient h_ϕ can be determined from:

$$h_\phi = [\rho_i L/(T_\infty - T_o)](\mathrm{d}b/\mathrm{d}t)_\phi. \quad (2)$$

Consequently, average heat transfer coefficient h_m can be written as:

$$h_m = \Sigma h_\phi A_\phi / \Sigma A_\phi. \quad (3)$$

The local melting velocity $(\mathrm{d}b/\mathrm{d}t)_\phi$ was evaluated by the ice contours which were recorded successively through photography, at designated time intervals.

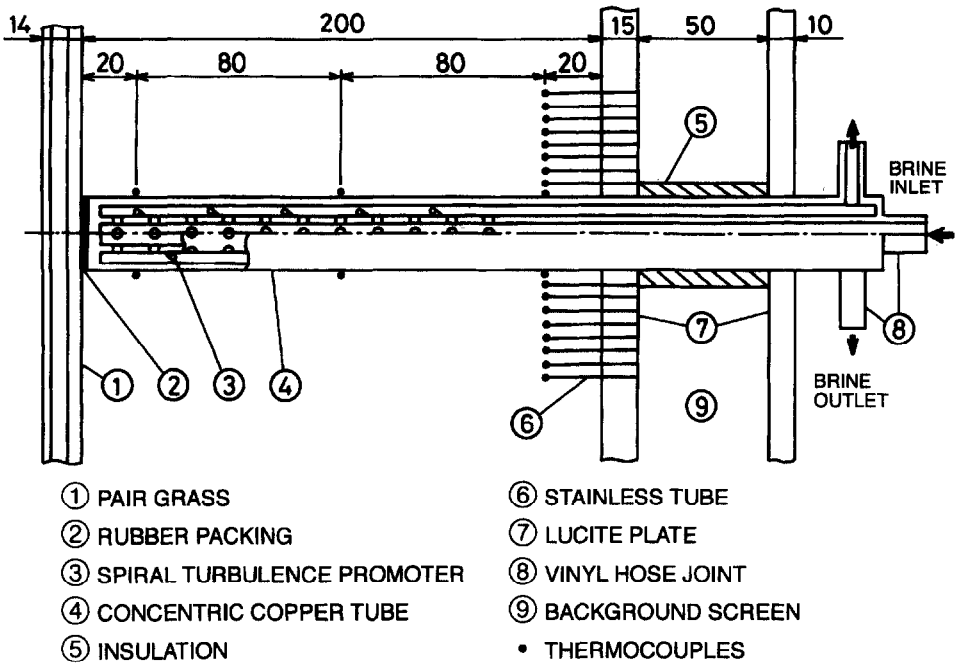

Fig. 2. Details of cooled cylinder.

3.3. *Relationship between ice–liquid interface temperature and ambient temperature*

Josberger and Martin [14] measured the ice–liquid interface temperature during the melting of a vertical ice plate in sea water and found that the temperature was not constant as observed for melting in pure water, but was a function of the ambient saline–water temperature. A similar phenomenon was observed during the melting of a horizontal circular ice cylinder immersed in quiescent saline water.

The measurement results of the ice–liquid interface temperature are presented in Fig. 3. The interface temperature T_o was determined by both the melting experiment of the small ice block within which the thermocouples were set and by the assumption of isothermal condition within the ice block. In the figure there are three groupings of the data which, respectively, correspond to ambient salinities of 0.5, 1.0 and 3.5 wt%. The ordinate variable is the dimensionless interface temperature $(T_o - T_{sp})/(T_{fp} - T_{sp})$, where T_{sp} denotes the freezing temperature of solvent in the solution and T_{fp} the fusion temperature of the solution. The abscissa variable is the dimensionless temperature difference between the ambient saline water temperature T_∞ and fusion temperature T_{fp}. In the figure, the previous data [14] for turbulent boundary layer flow are adopted for comparison.

Figure 3 shows that $(T_o - T_{sp})/(T_{fp} - T_{sp})$ decreases monotonically from near unity (where the ice is close to equilibrium with the ambient) to near-zero for any ambient salinity levels. This can be explained by considering that the melt water causes a decrease in the salinity of saline water just adjacent to the ice surface, which corresponds to an increase in fusion temperature. The present data might be correlated as a function of the ambient saline water concentration as follows:

$$T_o = T_{sp} + (T_{fp} - T_{sp}) \exp\left[-3.09 \times 10^{-1} (T_{fp} - T_\infty)/(T_{fp} - T_{sp})\right] \quad \text{for } S_\infty = 3.5\,\text{wt\%} \quad (4)$$

$$T_o = T_{sp} + (T_{fp} - T_{sp}) \exp\left[-6.87 \times 10^{-2} (T_{fp} - T_\infty)/(T_{fp} - T_{sp})\right] \quad \text{for } S_\infty = 1.0\,\text{wt\%} \quad (5)$$

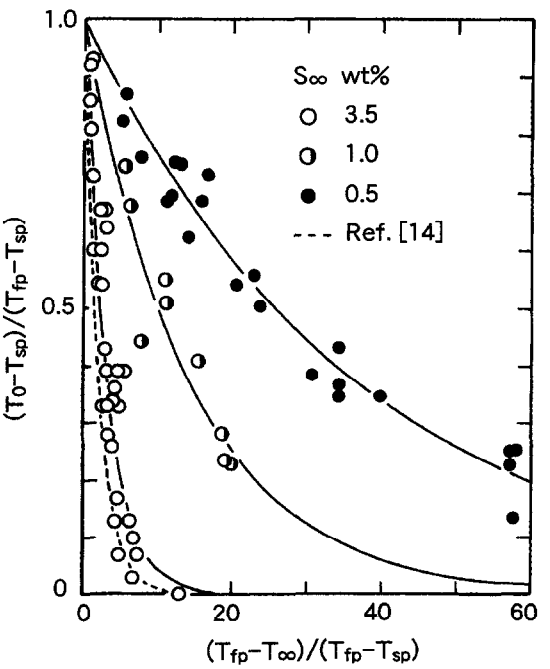

Fig. 3. Temperature of melting ice surface.

$$T_o = T_{sp} + (T_{fp} - T_{sp}) \exp [-2.68 \times 10^{-2}(T_{fp} - T_\infty)/(T_{fp} - T_{sp})] \quad \text{for } S_\infty = 0.5\,\text{wt\%}. \quad (6)$$

3.4. *Dimensionless groups*

A number of dimensionless groups will be employed in the presentation of the experimental results. By adopting the initial ice cylinder diameter D_{in} as the reference length, one defines an average Nusselt number as follows:

$$Nu_m = h_m D_{in}/\lambda_f \quad (7)$$

where the thermal conductivity λ_f is the arithmetic mean value $(\lambda_o + \lambda_\infty)/2$ of the interface and the ambient. In the present experiments, the ambient saline-water temperature T_∞ ranged from 1.8 to 24.0°C with the ambient salinity level S_∞ being between 0.5 and 3.5 wt% and the initial ice-cylinder diameter ranged from 85 to 90 mm. Thus, a modification is necessary, since the initial ice-cylinder diameter is not always the same throughout the experiments. The Nusselt number was divided by $(D_{in}/D_o)^{3/4}$ [23, 24], since the Nusselt number as defined by equation (7) is proportional to the reference length to the 3/4 power in the range where the boundary-layer approximation is valid. One defines the modified average Nusselt number by the following expression:

$$Nu_m^* = Nu_m (D_{in}/D_{sc})^{3/4} \quad (8)$$

where the reference diameter was taken as $D_{sc} = 100$ mm to compare with the previous data [19, 22, 23]. In addition, the Rayleigh number is defined as:

$$Ra = g(\rho_f - \rho_o) D_{in}^3/(\rho_\infty \nu a) \quad (9)$$

in which g is the acceleration of gravity. The thermophysical properties ν and a were evaluated at the arithmetic mean value of the interface and the ambient temperature.

4. RESULTS AND DISCUSSION

4.1. *Melting phenomena and flow patterns*

A number of data runs have been carried out to determine the effects of the ambient salinity level as well as the ambient temperature on the melting behavior and the flow structure. The results are presented in Fig. 4, in which the ordinate variable is the ambient temperature and the abscissa variable is the ambient salinity level. The measurements reveal that three distinct melting characteristics and flow regimes may be identified for both the ambient salinity level and the ambient temperature, which invoke variation in the melting feature of the horizontal ice cylinder corresponding, respectively, to the photographs of Figs. 5–7.

The regime I in Fig. 4, which corresponds to Fig. 5, agrees with the region where the density inversion of saline water occurs. As shown in Fig. 5, the deviation of the ice–liquid interface from the circular shape

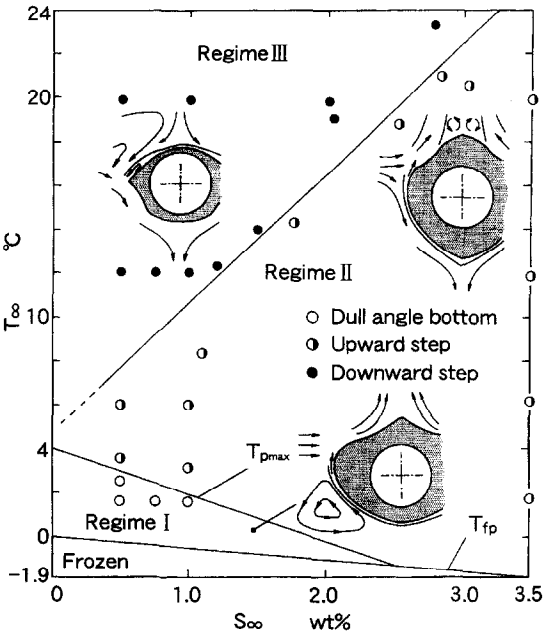

Fig. 4. Characteristics of melting ice profile.

results from strong free convection effects. It was observed that the flow around the melting ice cylinder was basically upward. At the lower portion of the ice cylinder the laminar velocity field is unidirectional, consisting of both a quite narrow melt flow and a wider outer saline water flow. The temperature of the outer upward saline water decreases along the ice cylinder, which then causes a decrease in the heat transfer coefficient. This may be the main reason for the increasing thickness of the ice layer in an upward direction. Along the upper portion of the ice cylinder, the velocity field is turbulent flow above the step, which probably results from the abrupt increase in the heat transfer coefficient due to the resultant convergence between an upward flow along the ice cylinder and a horizontal flow of ambient saline water flowing toward the ice cylinder. In addition to the fact mentioned above, it was observed that the location of the step tends to move upward as the ambient salinity level increases.

Figure 6 represents the melting characteristics and the flow structure observed in regime II in Fig. 4. Along the lower portion of the melting ice cylinder, the laminar velocity field is bidirectional, consisting of a quite narrow upward inner flow adjacent to the ice cylinder inside a wider downward outer flow. On the other hand, along the upper portion of the ice cylinder the velocity field is unidirectional and upward turbulent flow above the step, which may be due to the abrupt increase in the heat transfer coefficient at the transition point. At the level of transition to turbulence, it appears that the turbulent diffusion may transport both dilute saline water and upward momentum away from the ice over a horizontal distance comparable to the thermal boundary layer

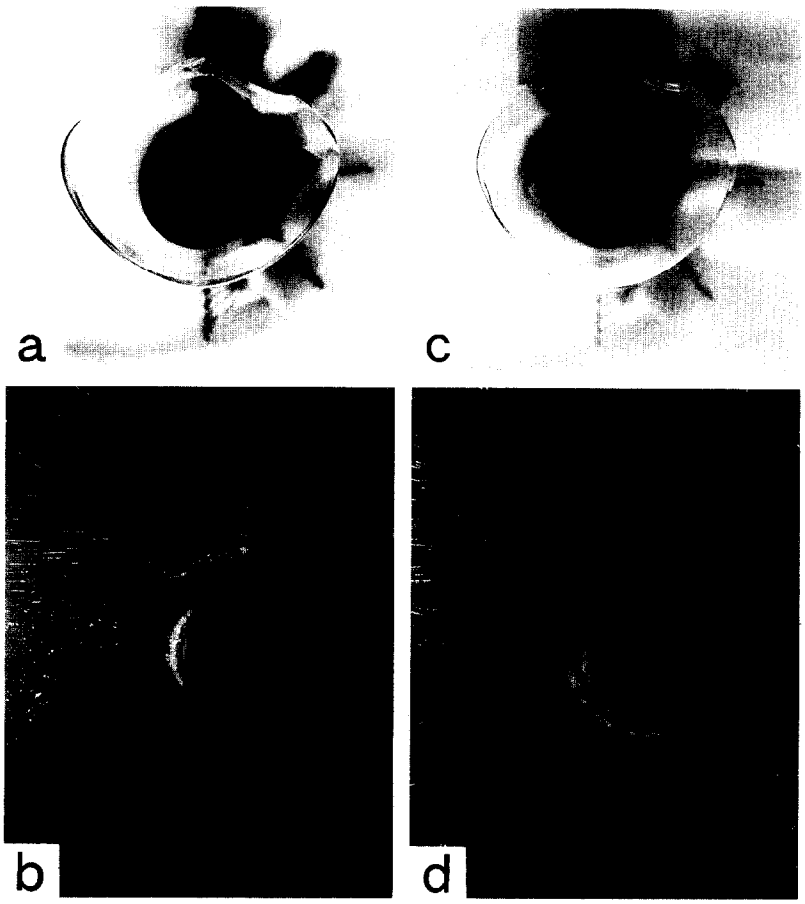

Fig. 5. Melting ice profile and flow pattern (T_∞ = 1.8°C, 300 min elapsed, regime I): (a, b) S_∞ = 1.0 wt%; (c, d) S_∞ = 0.8 wt%.

thickness. This upward buoyancy and momentum may overcome the downward buoyancy, such that the net result is an upward-flowing turbulent boundary layer. Then, it seems that the resultant divergence between the upward turbulent flow and the downward laminar thermal flow may produce a horizontal jet of ambient saline water flowing toward the ice cylinder. Similar phenomena were reported in [14] for the flow along a melting vertical ice plate. In addition, it was observed that the station of the step tended to move downward as the ambient salinity level increased. This may be due to the fact that the volumetric expansion coefficient of the saline water increases as the ambient salinity level increases, which promotes the upward flow along the ice cylinder at the lower portion of the cylinder.

The melting characteristics and the flow patterns, which were observed in the regime III in Fig. 4, are indicated in Fig. 7. The flow around the melting ice cylinder at the upper portion of the ice cylinder is basically downward, which is clearly in contrast to that of the regime I. At the lower portion of the ice cylinder the velocity field is bidirectional, consisting of both a narrow upward dilute saline water due to the melt just adjacent to the ice cylinder and a wider downward thermal flow. This upward buoyancy and momentum do not overcome the downward buoyancy such that the adverse flow (vortex) region takes place where the step tends to be observed (see Fig. 7). It was found that the station of the step tends to move downward as the ambient salinity level decreased. This fact is explained by considering that the buoyancy of the narrow upward dilute saline water may become weak owing to a decrease in ambient salinity level.

4.2. *Local heat transfer characteristics*

Figures 8–10 demonstrate the variation of the local heat transfer coefficient using the ambient salinity level as parameter. The abscissa variable is the angle ϕ from the top of the cylinder. The figures reveal that the local heat transfer characteristics are a quite strong function of the ambient salinity level. Figure 8 is for ambient saline water temperature T_∞ of 1.8°C with the advanced time of 240 min, corresponding to the regime I in Fig. 4. At the portion below the step the heat transfer decreases markedly, takes the minimum, then increases as the bottom of the cylinder is

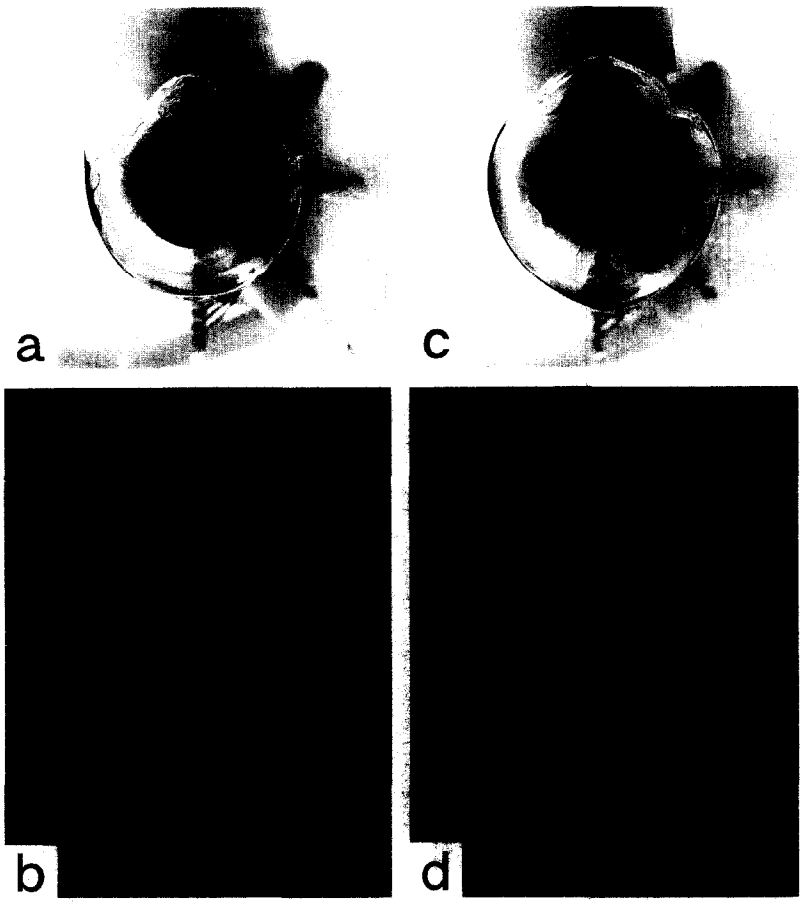

Fig. 6. Melting ice profile and flow pattern ($T_\infty = 6.1$°C, 50 min elapsed, regime II): (a, b) $S_\infty = 3.5$ wt%; (c, d) $S_\infty = 1.0$ wt%.

approached. This may be, as pointed out earlier, attributed to the fact that the temperature of the upward dilute saline water flow just adjacent to the ice cylinder decreases to reduce the melting rate.

In the regime II, there appears to be the maximum heat transfer coefficient just above the transition station, as shown in Fig. 9. This station tends to move upwards as the salinity level of the ambient liquid increases; for $S_\infty = 0.5$ wt% the maximum heat transfer coefficient is around $\phi = \pi/6$, while for $S_\infty = 3.5$ wt% it is around $\phi = \pi/3$. In addition, the heat transfer coefficient in general increases with an increase in the salinity level of the ambient liquid. The reason may be as follows: the buoyancy increases due to increasing density difference between the ambient fluid and the dilute salt water just adjacent to the ice cylinder; increasing salinity level of the ambient liquid reduces the temperature of the ice surface, which results in an increasing temperature difference between the ambient liquid and the ice cylinder surface.

Figure 10 presents the variation of the local heat transfer coefficient of the regime III in Fig. 4. It appears that the heat transfer coefficient may be minimum around just above the step. At the upper portion of the ice cylinder the temperature of the downward flow reduces along the cylinder, thus resulting in a decreasing temperature difference between T_0 and T_∞.

4.3. *Morphology of melting ice surface*

It was reported in [19] that for $S_\infty = 3.5$ wt% a variety of melting behavior of the melting ice cylinder surface was observed as a function of ambient temperature. Similar characteristics of the melting ice surface were also observed as a function of the ambient salinity level, as shown in Fig. 11.

In the regime I, the lower surface of the melting ice cylinder appears to be quite smooth [see Fig. 11(a)], while at the upper portion of the cylinder the ice surface develops circumferential groves with regular amplitude [see Fig. 11(b)], which terminate at the top of the cylinder because there is no separation point. The grooves probably result from the onset of the secondary flow within the upward flow.

In the regime II there occurs the separation point, above which the melting ice surface is quite similar to a surface scooped out by the spoon, as indicated in Fig. 11(c). The grooves with regular amplitude, whose

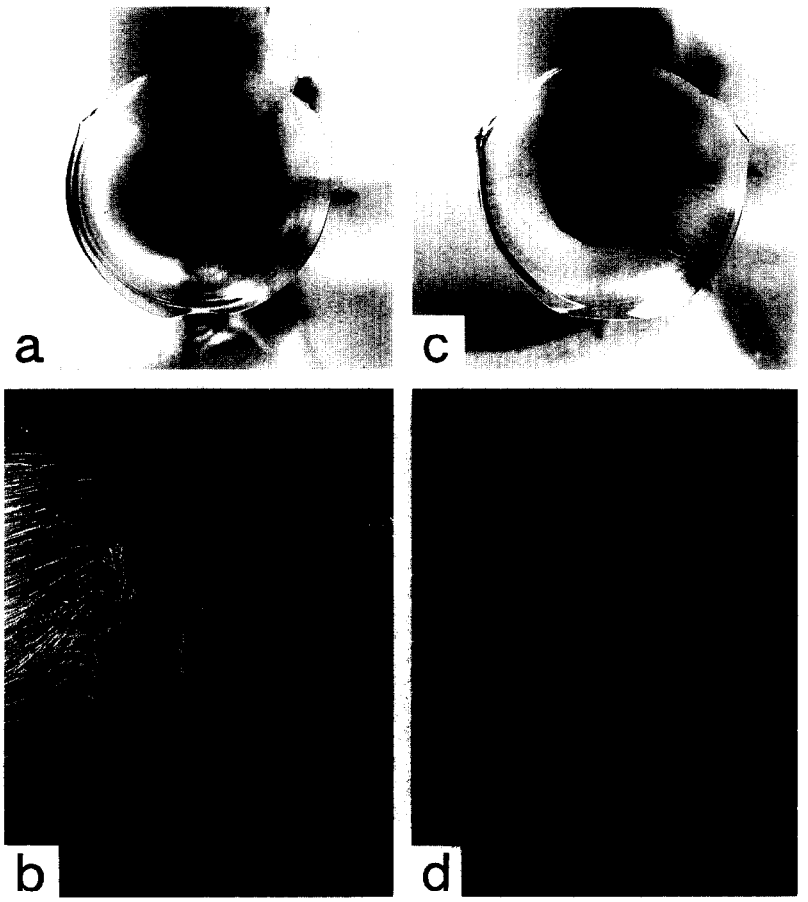

Fig. 7. Melting ice profile and flow pattern (T_∞ = 11.8°C, 20 min elapsed, regime III): (a, b) S_∞ = 1.0 wt%; (c, d) S_∞ = 0.5 wt%.

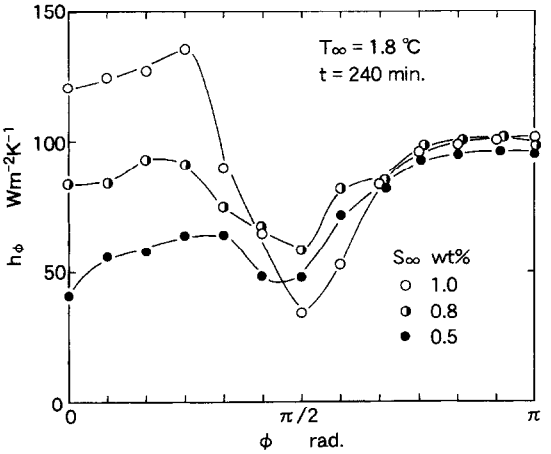

Fig. 8. Local heat transfer coefficient (regime I).

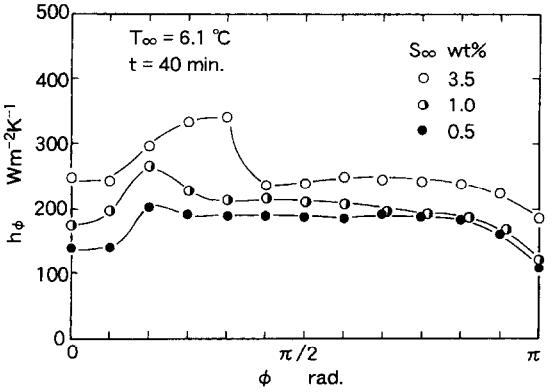

Fig. 9. Local heat transfer coefficient (regime II).

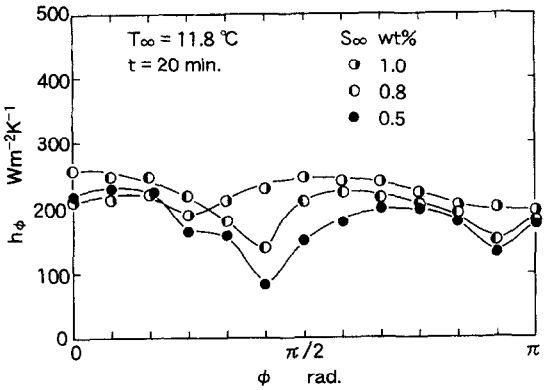

Fig. 10. Local heat transfer coefficient (regime III).

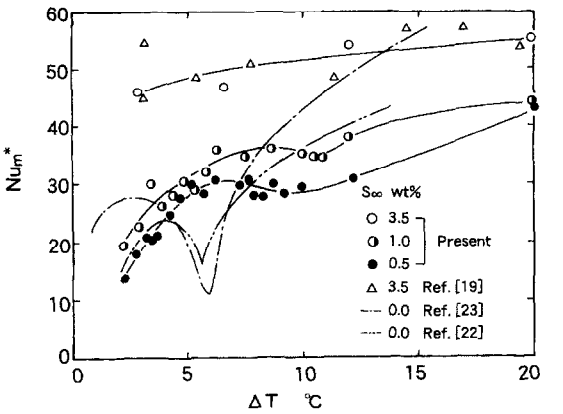

Fig. 12. Modified Nusselt number.

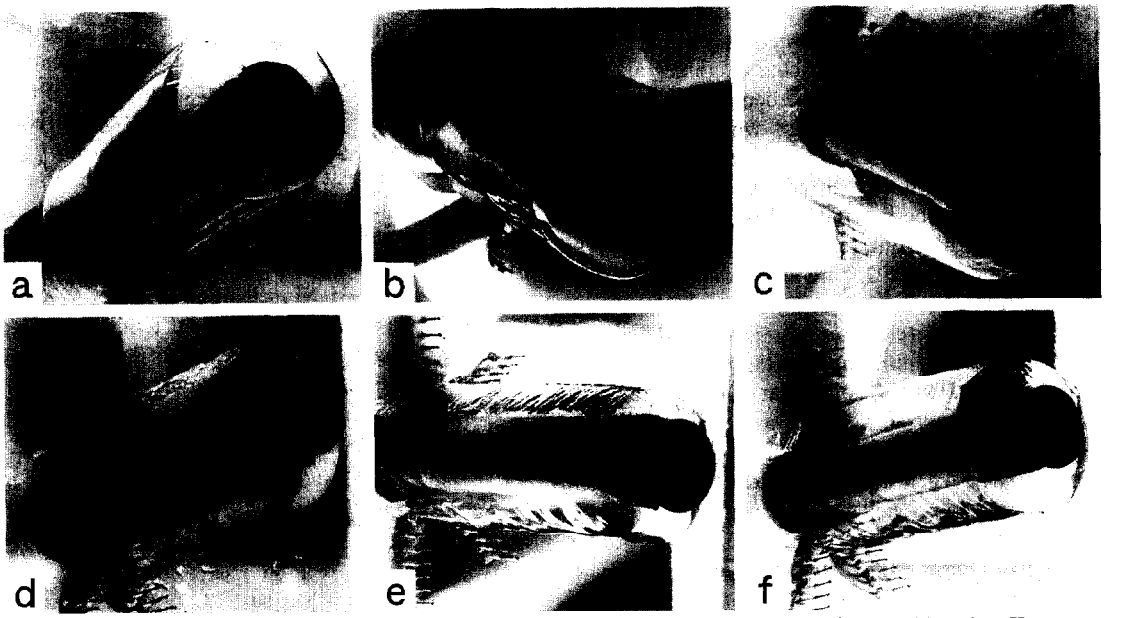

Fig. 11. Melting ice surface: (a, b) regime I, $T_\infty = 1.8°C$, $S_\infty = 0.5$ wt%, 360 min elapsed; (c) regime II, $T_\infty = 11.8°C$, $S_\infty = 3.5$ wt%, 12 min elapsed; (d) regime II, $T_\infty = 6.1°C$, $S_\infty = 1.0$ wt%, 10 min elapsed; (e) regime III, $T_\infty = 11.8°C$, $S_\infty = 1.0$ wt%, 32 min elapsed; (f) regime III, $T_\infty = 11.8°C$, $S_\infty = 1.0$ wt%, 24 min elapsed.

onset may be the same as that in the regime I, are observed from the step to the separation point. The ice surface at the lower portion of the ice cylinder for both the lower ambient salinity level and the lower ambient temperature appears to be rather smooth [see Fig. 11(d)].

In the regime III a number of quite small grooves are observed at the upper portion of the ice cylinder, as shown in Fig. 11(e). This may be due to the onset of secondary convection based on the interaction between the upward melt flow and the strong downward thermal flow. In addition, the similar grooves are also observed just below the step owing to the three-dimensional vortexes. Inversely, at the lower portion of the cylinder the smooth crests take place [see Fig. 11(f)]. This may be interpreted in terms of the bidirectional structure of the boundary layer flow. The flow is upward in the concentration (salinity) boundary layer, which is potentially stable, while the maximum density in the thermal boundary layer outside of the concentration boundary layer exists, which destabilizes the downward laminar flow. Therefore, the bidirectional flow is unstable for higher T_∞ and the onset of the secondary flow occurs, thus resulting in the uneven ice surface.

4.4. *Average heat transfer characteristics*

The average heat transfer characteristics are presented in Fig. 12. The ordinate denotes the modified average Nusselt number Nu_m^*, while the abscissa denotes the temperature difference between the ambient and the ice-cylinder surface ΔT $(=T_\infty - T_0)$. In the figure, the experimental results for melting heat transfer of the horizontal ice cylinder in seawater [19] and in pure water [22, 23] are also indicated for comparison. An inspection of the figure reveals that, as a whole, the Nu_m^* increases monotonically with increasing ΔT. However, more careful examination indicates that the heat transfer somewhat decreases around $\Delta T = 7$–$9°C$ and 9–11°C for $S_\infty = 0.5$ and 1.0 wt%, respectively. The temperature difference ΔT may be approximated when T_{fp} is much less than T_∞. Then the ΔT value, mentioned above, corresponds approximately to the ambient temperature T_∞ of the border between the regime II and the regime III in Fig. 4. Namely, it seems that at that temperature, the density of the fluid adjacent to the melting ice cylinder may become equal to that of the ambient fluid, thus yielding a decrease in convection effect in heat transfer.

Figure 13 represents the relationship between the modified average Nusselt number and the Rayleigh number. A best fit throughout the present data yields the final equation in the form

$$Nu_m^* = 8.05 \times 10^{-2} Ra^{0.32} \quad (3 \times 10^7 \leqslant Ra \leqslant 10^9). \tag{10}$$

5. CONCLUSIONS

The effect of salinity level on the melting characteristics of a horizontal circular cylinder immersed in quiescent saline water were determined. The following conclusions may be drawn within the parameters covered.

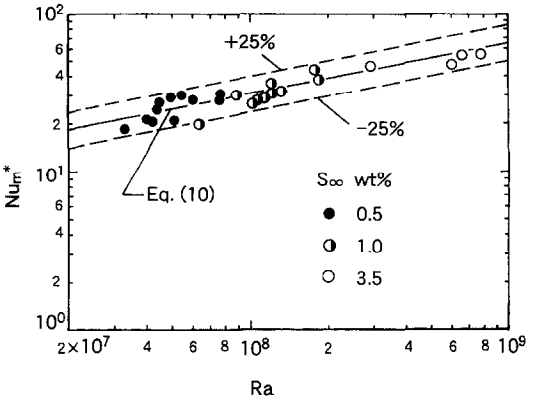

Fig. 13. Modified Nusselt number.

(1) Three distinct melting characteristics and flow regimes are identified as a function of both the ambient fluid salinity level and the ambient fluid temperature.

(2) At the upper portion of the melting ice cylinder the grooves with regular amplitude are observed for any thermal conditions. On the other hand, at the lower portion of the cylinder the ice surface in the regimes I and II is smooth, while in the regime III the crests with long regular amplitude take place.

(3) The local heat transfer coefficient tends to take the minimum just below the step in the regime I, the maximum just above the step in the regime II and the minimum just above the step in the regime III.

(4) The modified Nusselt number tends to somewhat decrease at a certain ambient temperature like that for melting in pure water, but its decreasing rate is much less than that for pure water.

REFERENCES

1. Viskanta, R., Heat transfer during melting and solidification of metals. *Transactions of the ASME Journal of Heat Transfer*, 1988, **110,** 1205–1219.
2. Yao, L. S. and Prusa, J., Melting and freezing. *Advances in Heat Transfer*, 1990, **19,** 1–95.
3. Fukusako, S. and Yamada, M., Recent advances in research on water-freezing and ice-melting problems. *Experimental Thermal and Fluid Science*, 1994, **6,** 90–105.
4. Fukusako, S. and Yamada, M., Recent advances in research on melting heat transfer problems. *Proceedings of the 10th International Heat Transfer Conference*, 1994, **1,** 313–331.
5. Neshyba, S., Upwelling by icebergs. *Nature*, 1977, **267,** 507–508.
6. Huppert, H. E. and Turner, J. S., On melting icebergs. *Nature*, 1978, **27,** 46–48.
7. Greisman, P., On upwelling driven by the melt of ice shelves and tidewater glaciers. *Deep-Sea Research*, 1979, **26,** 1051–1065.
8. Marshall, E., Free convection melting on glacial ice in saline water. *Letters of Heat and Mass Transfer*, 1977, **4,** 381–384.
9. Martin, S. and Kauffman, P., An experimental and

theoretical study of the turbulent and laminar convection generated under a horizontal ice sheet floating on warm salty water. *Journal of Physics and Oceanology*, 1977, **7**, 272–283.
10. Gade, H. G., Melting of ice in sea water: a primitive model with application to the Antarctic ice shelf and ice bergs. *Journal of Physics and Oceanology*, 1979, **9**, 189–198.
11. Huppert, H. E. and Turner, J. S., The melting of ice in cold stratified water. *Journal of Physics and Oceanology*, 1980, **10**, 953–960.
12. Josberger, E. G., The effect of bubbles released from a melting ice wall on the melt-driven convection in salt water. *Journal of Physics and Oceanology*, 1980, **10**, 474–477.
13. Huppert, H. E. and Turner, J. S., Ice blocks melting into a salinity gradient. *Journal of Fluid Mechanics*, 1980, **100**, 367–384.
14. Josberger, E. G. and Martin, S., A laboratory and theoretical study of the boundary layer adjacent to a vertical ice wall in salt water. *Journal of Fluid Mechanics*, 1981, **111**, 439–473.
15. Carey, V. P. and Gebhart, B., Transport near a vertical ice surface melting in saline water: experiments at low salinities. *Journal of Fluid Mechanics*, 1982, **117**, 403–423.
16. Sammakia, B. and Gebhart, B., Transport near a vertical ice surface melting in water of various salinity levels. *International Journal of Heat and Mass Transfer*, 1983, **26**, 1452–1493.
17. Johnson, R. S. and Mollendorf, J. C., Transport from a vertical ice surface melting in saline water. *International Journal of Heat and Mass Transfer*, 1984, **27**, 1928–1932.
18. Qureshi, Z. H. and Gebhart, B., The stability of vertical thermal buoyancy induced flows in cold pure and saline water. *International Journal of Heat and Mass Transfer*, 1986, 1383–1392.
19. Fukusako, S., Tago, M., Yamada, M., Kitayama, K. and Watanabe, C., Melting heat transfer from a horizontal ice cylinder immersed in quiescent saline water. *Transactions of the ASME Journal of Heat Transfer*, 1992, **114**, 34–40.
20. Fukusako, S., Yamada, M., Horibe, A. and Watanabe, C., Melting characteristics of a horizontal ice cylinder immersed in saline water: effect of liquid depth to saline water surface. ASME paper HTD-271, 1994, 81–87.
21. Fukusako, S., Yamada, M. and Watanabe, C., Melting characteristics of ice blocks immersed in quiescent saline water. *Annals Glaciology*, 1994, **19**, 126–130.
22. Kishinami, K., Saito, S. and Tokura, I., Study of free convection heat transfer from a horizontal ice cylinder immersed in quiescent pure water. *Preprints of 50th JSME Annual Meeting*, 1972, 251–254.
23. Saitoh, T., Natural convection heat transfer from a horizontal ice cylinder. *Applied Science Research*, 1976, **32**, 429–451.
24. Cheng, K. C., Inaba, H. and Gilpin, R. R., Effects of natural convection on ice formation around an isothermally cooled horizontal cylinder. *Transactions of the ASME Journal of Heat Transfer*, 1988, **110**, 931–937.